Journal of Applied Electrochemistry **33**: 853–862, 2003.

Simultaneous recovery of Pb and PbO_2 from battery plant effluents. Part II☆

N.P. BRANDON[1], D. PILONE[1,2], G.H. KELSALL[1,]* and Q. YIN[1]
[1]*Department of Chemical Engineering and Chemical Technology, Imperial College, London SW7 2BY, Great Britain*
[2]*Università degli Studi di Roma, 'La Sapienza', Roma, Italy*
*(*author for correspondence, e-mail: g.kelsall@ic.ac.uk)*

Received 29 November 2002; accepted in revised form 8 April 2003

Key words: felt electrodes, lead, lead(II), lead dioxide, oxidation, reduction

Abstract

Results are reported of experiments and modelling of cathodic Pb and anodic PbO_2 electrodeposition, aimed at developing a process using both reactions simultaneously for treating aqueous effluents from lead–acid battery recycling plants. Pb(II) solubilities and equilibrium potentials were calculated as functions of pH and sulfate activities. Using kinetic parameters from the literature or determined experimentally, models were developed for current density–potential and current efficiency–potential relationships, together with the current density dependence of specific electrical energy consumptions for Pb(II) recovery. Experimental current density–potential and charge efficiency–potential relationships were in broad agreement with model predictions, with near unity current efficiencies for mass transport controlled PbO_2 deposition from electrolytes containing 1 mol Pb(II) m^{-3} at pH 12. However, charge efficiencies for cathodic deposition of lead were typically 0.2 for 1 mol Pb(II) m^{-3} + 1 mol O_2 (aq) m^{-3}; removal of dissolved oxygen was predicted and determined to increase current efficiencies to near unity. Pb(II) concentrations were depleted to <60 ppb in a batch recycle reactor system with graphite felt anodes and graphite or titanium felt cathodes. Simultaneous cathodic Pb and anodic PbO_2 electrodeposition resulted in more rapid Pb(II) depletion than for either reaction separately.

List of symbols

a	specific electrode area (m^{-1})
A	electrode cross-sectional area (m^2)
B	inverse Tafel slope (V^{-1})
c	crystalline (–)
c_i	electrolyte concentration of species i (mol m^{-3})
D_i	diffusion coefficient of species i (m^{2+} s^{-1})
E	electrode potential vs reference electrode (V)
E^0	equilibrium electrode potential under standard conditions vs reference electrode (V)
E_r	equilibrium electrode potential vs reference electrode (V)
f	disc electrode rotation rate (s^{-1})
F	faraday constant (96 485 C mol^{-1})
g	interelectrode gap (m^{2+})
j	current density (A m^{-2})
j_L	mass transport controlled current density (A m^{-2})
j_0	exchange current density (A m^{-2})
k_m	mass transport rate coefficient (m s^{-1})
k_0	standard heterogeneous reaction rate coefficient (m s^{-1})
L	length of porous electrode in direction of current flow (m)
M	molar mass (g mol^{-1})
n_i	charge number of reaction for rate determinate step (number of moles of electrons per mole of electroactive species)
R	gas constant (8.31441 J mol^{-1} K^{-1})
T	time (s)
T	absolute temperature (K)
U	electrolyte flow rate (M^3 s^{-1})
U	electrochemical reactor terminal voltage (V)
u	electrolyte velocity (m^3 s^{-1})
V	electrolyte volume (m^3)
X_t	time-dependent fractional conversion of reactant
z_i	number of elementary charges on ionic species i
α	transfer coefficient for reaction
α-PbO_2	orthorhombic PbO_2 (–)
β-PbO_2	tetragonal PbO_2 (–)
δ	diffusion layer thickness (m)
ϕ	potential (V)

☆ This paper was originally presented at the 6th European Symposium on Electrochemical Engineering, Düsseldorf, Germany, September 2002.

Φ	(fractional) current efficiency
σ	electrolyte specific conductivity, $F\sum_i z_i u_i c_i$ (S m^{-1})
η	overpotential (E–E_r) (V)
υ	electrolyte kinematic viscosity (m^2 s^{-1})

1. Introduction

Both the manufacture and recycling of lead acid batteries generate aqueous effluents containing low concentrations of Pb(II) species, for which the consent concentrations for permitted discharge to sewers are in the range from a few ppm down to zero, depending on the country, though the upper limits are likely to be decreased by environmental agencies in the future. Present industrial practice involves treating such Pb(II)-containing effluents with lime to precipitate a mixture of lead sulfate, hydroxides and gypsum, which may then be sent to a landfill site, though this route is likely to be precluded by future legislation, because of possible mobilization of the Pb(II) contaminated water-courses. As shown schematically in Figure 1, lead–acid battery recycling plants coupled to smelters [1] use sodium hydroxide to neutralize residual sulfuric acid and desulfurise discharged battery paste, thereby avoiding SO_2 emissions from smelters, the sulfate being discharged as aqueous sodium sulfate, possibly containing some residual dissolved Pb(II) together with colloidal particles. Hence, the need to develop novel processes for recovering such Pb(II) species.

The anions perchlorate, nitrate, tetrafluoroborate, sulfate and chloride have been reported [2] to have a marked influence on electrodeposition kinetics and current efficiencies for Pb(II) reduction at a reticulated vitreous carbon (RVC) cathode. Only in chloride electrolytes was the reaction mass transport controlled, slower kinetics being exhibited in the other electrolyte solutions. The anion effect was attributed to the slow steps in the nucleation and/or early growth of the lead deposition on the carbon surface in the first three electrolytes, while in sulfate media, it was attributed to surface poisons and passivating layer formation.

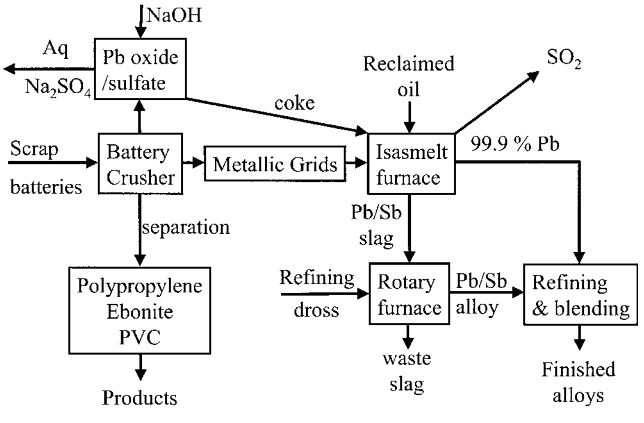

Fig. 1. Process flow sheet for 55 ktonne p.a. lead acid battery recycling process, Britannia Refined Metals Ltd, Northfleet, UK.

The electrochemical behaviour of lead and lead dioxide deposited on reticulated vitreous carbon has also been investigated [3,4] in 0.1 M NaOH, 0.1 M $Na_2B_4O_7$ and 0.5 M H_2SO_4, the behaviour of the electrodeposits being almost identical to that of metallic lead or lead coated with lead dioxide. However, the behaviour of the PbO_2 electrode in borate solutions was found to be more sensitive than that of lead and there were significant effects of platinising the RVC matrix on PbO_2 deposition.

A flow-through reticulated vitreous carbon cathode has also been used [5] for electrolytic removal/recovery of Pb(II) from borate/nitrate solutions, at potentials determined from kinetic measurements with a vitreous carbon rotating disc electrode. As expected, the removal rate increased as the electrode porosity and flow rate were increased, the Pb(II) concentration being decreased to 0.1 ppm in 20 min to 2 h, with a cathode to catholyte volume ratio of 0.027.

A stack of copper screens has been used [6] to form a three dimensional cathode for electrodeposition of lead ions, the transport limited current increasing, as expected, with their concentration, electrolyte flow rate, and/or electrode thickness. Cyclic voltammetry and atomic force microscopy have been used to study [7] anion effects on Pb(II) removal from aqueous solution using a reticulated vitreous carbon electrode. Higher removal efficiencies were achieved in the case of chloride-containing electrolytes, and lowest efficiencies were achieved in sulfate electrolytes, which were believed to inhibit reduction by formation of a passivating surface film, in agreement with previous work [2].

None of these publications report using the approach advocated here, in which an electrochemical process [8] is being developed for lead recovery by simultaneous cathodic deposition of elemental Pb:

$$\Phi_{Pb}(Pb^{2+} + 2e^- \rightarrow Pb) \tag{1}$$

and anodic deposition of lead dioxide:

$$\Phi_{PbO_2}(Pb^{2+} + 2H_2O \rightarrow PbO_2(c, \beta) + 4H^+ + 2e^-) \tag{2}$$

where Φ_{Pb} and Φ_{PbO_2} represent fractional current efficiencies at graphite felt cathodes and anodes, respectively. The loss reactions are primarily,
at the cathode:

$$\Phi_{C,O_2}(0.5O_2 + 2H^+ + 2e^- \rightarrow H_2O) \tag{3}$$

$$\Phi_{H_2}(2H^+ + 2e^- \rightarrow H_2) \tag{4}$$

and at the anode:

$$\Phi_{A,O_2}(H_2O \rightarrow 0.5O_2 + 2H^+ + 2e^-) \tag{5}$$

Hence, the overall chemical change in the reactor is:

$$\begin{aligned}\mathrm{Pb}^{2+} &+ \left(\frac{2\Phi_{\mathrm{PbO_2}} + \Phi_{\mathrm{A,O_2}} - \Phi_{\mathrm{C,O_2}}}{\Phi_{\mathrm{Pb}} + \Phi_{\mathrm{PbO_2}}}\right)\mathrm{H_2O} \\ &+ 2\left(\frac{\Phi_{\mathrm{H_2}} + \Phi_{\mathrm{C,O_2}} - 2\Phi_{\mathrm{PbO_2}} - \Phi_{\mathrm{A,O_2}}}{\Phi_{\mathrm{Pb}} + \Phi_{\mathrm{PbO_2}}}\right)\mathrm{H^+} \\ &+ 0.5\left(\frac{\Phi_{\mathrm{C,O_2}} - \Phi_{\mathrm{A,O_2}}}{\Phi_{\mathrm{Pb}} + \Phi_{\mathrm{PbO_2}}}\right)\mathrm{O_2} \rightarrow \left(\frac{\Phi_{\mathrm{Pb}}}{\Phi_{\mathrm{Pb}} + \Phi_{\mathrm{PbO_2}}}\right)\mathrm{Pb} \\ &+ \left(\frac{\Phi_{\mathrm{PbO_2}}}{\Phi_{\mathrm{Pb}} + \Phi_{\mathrm{PbO_2}}}\right)\mathrm{PbO_2} + \left(\frac{\Phi_{\mathrm{H_2}}}{\Phi_{\mathrm{Pb}} + \Phi_{\mathrm{PbO_2}}}\right)\mathrm{H_2} \qquad (6)\end{aligned}$$

Such a process would be more elegant than the present industrial practice of treating lead effluents from battery production plants with various sources of hydroxide ions.

However, as explained above, for lead–acid battery recycling plants, alkaline electrolytes would be more appropriate, involving the following process chemistry: Anode

$$\Phi_{\mathrm{PbO_2}}(\mathrm{HPbO_2^-} + \mathrm{OH^-} \rightarrow \mathrm{PbO_2}(\mathrm{c},\alpha) + \mathrm{H_2O} + 2\mathrm{e^-}) \qquad (7)$$

Anode

$$\Phi_{\mathrm{A,O_2}}(2\mathrm{OH^-} \rightarrow 0.5\mathrm{O_2} + \mathrm{H_2O} + 2\mathrm{e^-}) \qquad (8)$$

Cathode

$$\Phi_{\mathrm{Pb}}(\mathrm{HPbO_2^-} + \mathrm{H_2O} + 2\mathrm{e^-} \rightarrow \mathrm{Pb} + 3\mathrm{OH^-}) \qquad (9)$$

Cathode

$$\Phi_{\mathrm{C,O_2}}(0.5\mathrm{O_2} + \mathrm{H_2O} + 2\mathrm{e^-} \rightarrow 2\mathrm{OH^-}) \qquad (10)$$

Cathode

$$\Phi_{\mathrm{H_2}}(2\mathrm{H_2O} + 2\mathrm{e^-} \rightarrow \mathrm{H_2} + 2\mathrm{OH^-}) \qquad (11)$$

resulting in the overall process chemistry:

$$\begin{aligned}\mathrm{HPbO_2^-} &+ \left(\frac{\Phi_{\mathrm{H_2}}}{\Phi_{\mathrm{Pb}} + \Phi_{\mathrm{PbO_2}}}\right)\mathrm{H_2O} \rightarrow \left(\frac{\Phi_{\mathrm{Pb}}}{\Phi_{\mathrm{Pb}} + \Phi_{\mathrm{PbO_2}}}\right)\mathrm{Pb} \\ &+ \left(\frac{\Phi_{\mathrm{PbO_2}}}{\Phi_{\mathrm{Pb}} + \Phi_{\mathrm{PbO_2}}}\right)\mathrm{PbO_2} + \left(\frac{\Phi_{\mathrm{H_2}}}{\Phi_{\mathrm{Pb}} + \Phi_{\mathrm{PbO_2}}}\right)\mathrm{H_2} \\ &+ 2\left(\frac{\Phi_{\mathrm{H_2}} + \Phi_{\mathrm{PbO_2}}}{\Phi_{\mathrm{Pb}} + \Phi_{\mathrm{PbO_2}}}\right)\mathrm{OH^-} + 0.5\left(\frac{1 - \Phi_{\mathrm{C,O_2}} - \Phi_{\mathrm{PbO_2}}}{\Phi_{\mathrm{Pb}} + \Phi_{\mathrm{PbO_2}}}\right)\mathrm{O_2} \\ &\qquad (12)\end{aligned}$$

The objective of the work, results of which are reported here, was to establish the feasibility of the coupled reactions in alkaline electrolytes in a single electrochemical reactor.

2. Experimental details

A rotating Pt (0.283 cm^2) disc electrode (Pine Instrument Company, PA) was used to investigate the electrode kinetics and charge efficiencies of Pb(II) reduction and oxidation, as functions of Pb(II) concentration, dissolved oxygen concentration, pH, and type and concentration of anion. Prior to experiments, the electrode was polished with aqueous dispersions of 300 nm alumina powder and then thoroughly washed with high purity water to remove any adhering particles.

All electrolytes were prepared from analytical grade chemicals and high purity water made by reverse osmosis (Elga Elgastat) and deionization (Elga Prima) to give a resistivity of 1.6×10^5 Ω m. The electrochemical experiments were carried out in a three compartment glass cell, incorporating a 6.5 cm^2 Pt sheet counter electrode and saturated calomel reference electrode (SCE), assumed to have a potential of 0.245 V vs SHE. The cathodic reduction experiments involved prepurging the electrolyte and cell with zero grade nitrogen or oxygen (BOC Gases Ltd) for at least half an hour to desorb dissolved oxygen or saturate with oxygen; during experiments, nitrogen or oxygen was flowed over the electrolyte surface. Electrochemical measurements were made with an Autolab Model PGstat 100 potentiostat/galvanostat (Eco Chemie BV, Netherlands) controlled by a computer.

As shown schematically in Figure 2, the (polypropylene) tubular electrochemical reactor was used for Pb(II) depletion experiments in batch recycle mode, with the flexibility to incorporate a (cation-permeable) membrane, such as Nafion® (DuPont), to enable the behaviour of cathode and anode to be investigated separately. Annular Ti plate feeder electrodes were used, initially with one or more discs of 6.3 mm thick graphite felt (RVG2003, Le Carbone (Great Britain)), with a bulk density of 0.1 g cm^{-3}, voidage of 0.94, (BET) surface area of 64 000 m^2 m^{-3}, cross-sectional area of 2.1×10^{-3} m^2 and interfacial surface area of 0.81 m^2. Latterly, a Ti felt (Bekaert SA, Belgium) cathode was used with a specific surface area of 3.3×10^3 m^{-1} and porosity of 0.96, calculated from the mass and strand diameter, giving an interfacial surface area of 4.4×10^{-2} m^2.

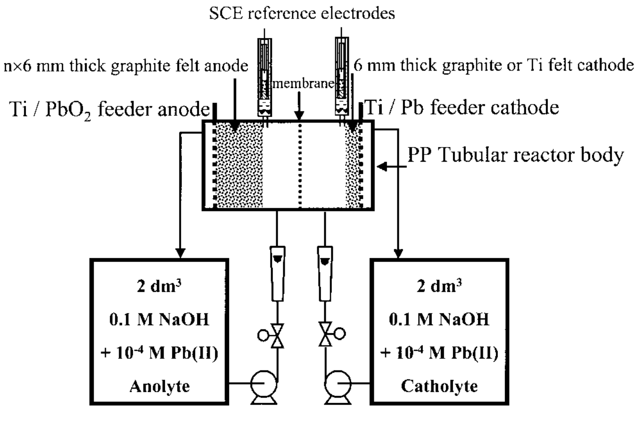

Fig. 2. Batch recycle reactor system for electrodeposition of Pb and PbO$_2$ on felt electrodes from aqueous Pb(II) electrolytes.

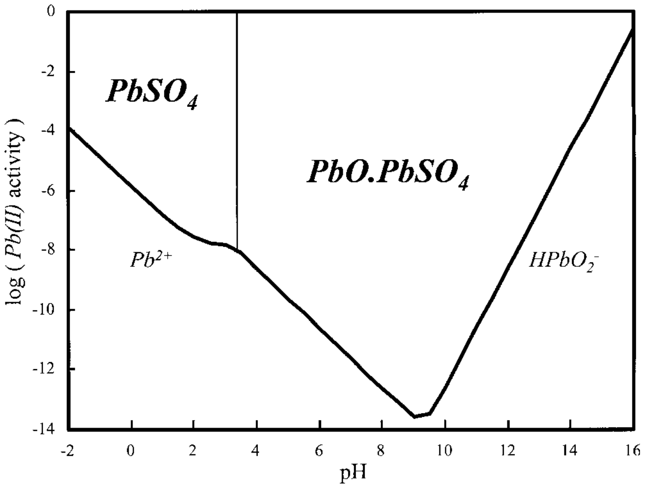

Fig. 3. Activity-pH diagram for Pb(II) species in equilibrium with $PbSO_4$ and $PbO/PbSO_4$ at 298 K.

Subsequently, the membrane was removed and, with a single reservoir and pump, the electrolyte was flowed through the reactor from cathode feeder to anode feeder, to minimise the amount of dissolved oxygen evolved at the anode from reaching the cathode, prior to recirculation of the electrolyte, which could be purged with nitrogen if required.

3. Results and discussion

3.1. *Thermodynamics of lead sulfate-water systems*

Figure 3 shows an activity–pH diagram for the Pb(II) sulfate–water system for unity dissolved sulfate activity. This was calculated from published [9], critically-assessed data, which, unlike the NBS compilation [10], lists only one of several phases related to $PbO \cdot PbSO_4$ that exhibits a predicted minimum Pb(II) solubility of $<10^{-13}$ M at about pH 9.5. However, when aqueous NaOH or $Ca(OH)_2$ is added to $PbSO_4$ to neutralize residual H_2SO_4, measured Pb(II) concentrations suggest that $PbSO_4$ transforms to $Pb(OH)_2$ rather than $PbO \cdot PbSO_4$, as the formation of the latter phase is presumably slow. Hence, Figure 4 was calculated, excluding $PbSO_4 \cdot PbO$ and PbO phases, revealing a $PbSO_4$/$Pb(OH)_2$ metastable equilibrium in the pH range 8.5–12, depending on the free sulfate activity. The resulting predicted Pb(II) activities are significantly greater than in Figure 3, so that, depending on free sulfate activities, dissolved Pb(II) discharge consent concentrations of about 1 ppm may not be met under the mildly alkaline conditions needed to effect the desulfurizing reaction:

$$PbSO_4\ (c) + 2OH^- \rightleftharpoons Pb(OH)_2\ (c) + SO_4^{2-} \qquad (13)$$

$$pH = 10.74 + 0.5\log(SO_4^{2-}) \qquad (14)$$

Figure 5 shows the corresponding metastable potential–pH diagram, having excluded $PbSO_4 \cdot PbO$, PbO, $PbO_{1.57}$ (c), Pb_3O_4 (c) and Pb_2O_3 (c) from the calculations, and drawn for a Pb(II) activity of 10^{-4} M, at which no $Pb(OH)_2$ (c) was formed by Reaction 13, the $PbSO_4$ (c) dissolving by the reaction:

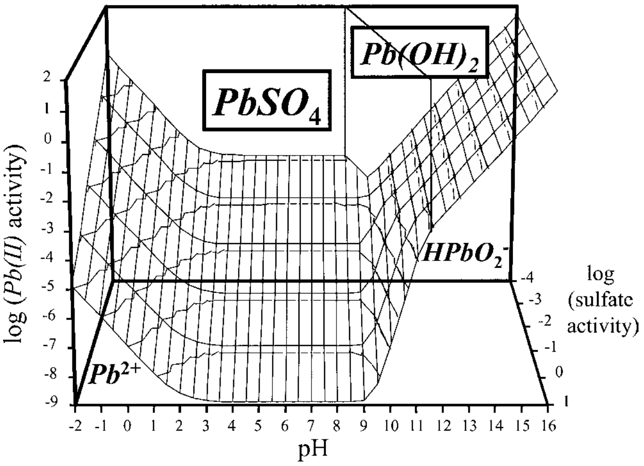

Fig. 4. Predicted solubility of Pb(II) species in metastable equilibrium with $PbSO_4$ (c) or $Pb(OH)_2$ (ppt.) in aqueous sulfate media at 298 K (excluding $PbO \cdot PbSO_4$ and PbO).

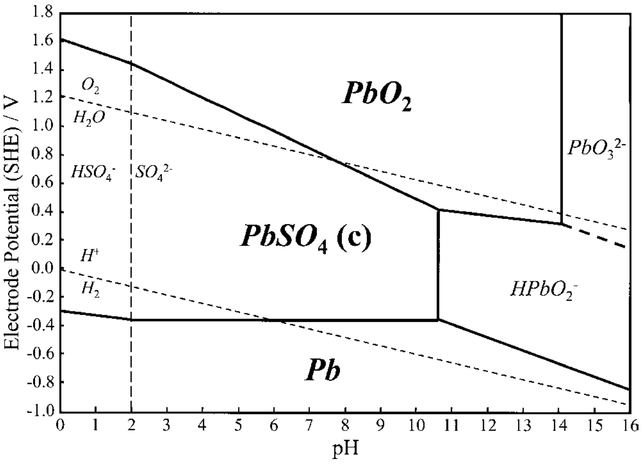

Fig. 5. Metastable potential–pH diagram for Pb-sulfate–H_2O system at 298 K and dissolved lead activity of 10^{-4} M.

$$PbSO_4\ (c) + 3OH^- \rightleftharpoons HPbO_2^- + H_2O + SO_4^{2-} \qquad (15)$$

$$\log(HPbO_2^-) = -35.84 + 3pH - \log(SO_4^{2-}) \qquad (16)$$

Figure 5 appears to provide better predictions of the kinetic behaviour of the system in acidic and alkaline solutions, the latter described below. A fuller report of thermodynamics of lead–water systems will be published later [11].

The proposed process for treating effluent from battery recycling processes (Figure 1) involves the cathodic reaction:

$$HPbO_2^- + H_2O + 2e^- \rightleftharpoons Pb + 3OH^- \qquad (9)$$

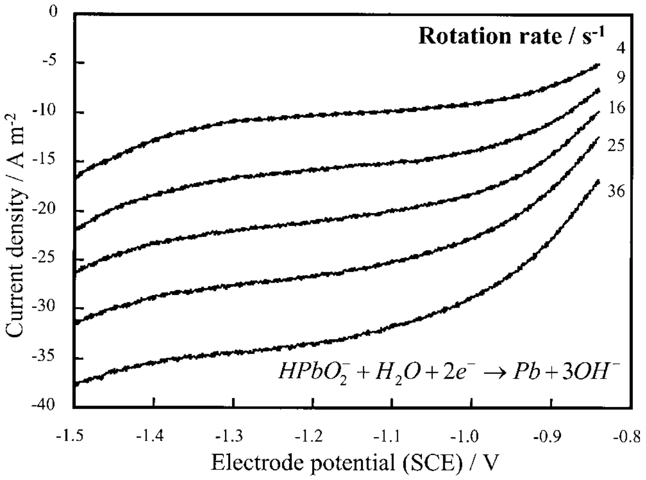

Fig. 6. $HPbO_2^-$ reduction at rotating Pt/PbO_2 disc electrode in 2 mol $HPbO_2^-$ + 100 mol OH^- m^{-3} at pH 13; potential sweep rate 100 mV s^{-1}.

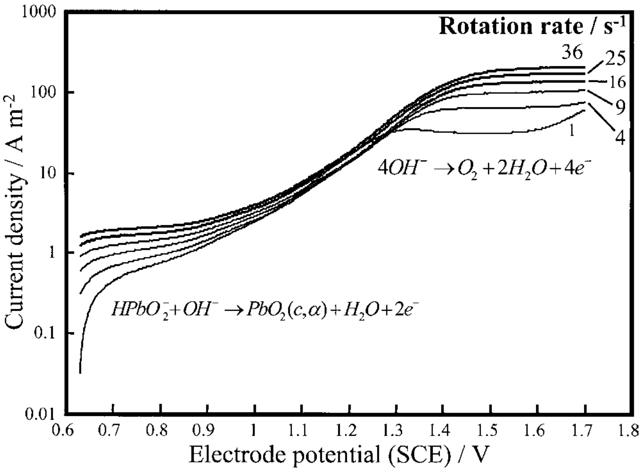

Fig. 7. $HPbO_2^-$ oxidation at rotating Pt/PbO_2 disc electrode in 0.1 mol $HPbO_2^-$ + 10 mol OH^- m^{-3} at pH 12. Voltammograms of (Pt/) PbO_2 disc electrode in 10^{-4} M $Pb(NO_3)_2$ + NaOH + $NaNO_3$ electrolyte of pH 12 and ionic strength 0.5; sweep rate 0.05 V s^{-1}.

$$E(\mathrm{SHE})/\mathrm{V} = 0.701 - 0.0887\,pH + 0.0296\log(HPbO_2^-) \quad (17)$$

coupled to the anodic reaction:

$$\mathrm{PbO_2\ (c) + H_2O + 2e^- \rightleftharpoons HPbO_2^- + OH^-} \quad (7)$$

$$E(\mathrm{SHE})/\mathrm{V} = 0.622 - 0.0296\,pH - 0.0296\log(HPbO_2^-) \quad (18)$$

subject to Pb(II) solubility constraints (Figure 4).

3.2. *Electrode kinetics*

Figure 6 shows a set of voltammograms for Pb(II) reduction at a Pt rotating disc electrode. As expected for a very fast reaction, with decreasing potential below the equilibrium potential of about −0.73 V vs SCE, current densities increased rapidly, reaching mass transport controlled conditions in the potential range −1.0 to −1.3 V vs SCE, below which hydrogen evolution partial current densities became significant. As the real surface area of the Pb deposits changed significantly with time, even at low Pb(II) concentrations, (pseudo-) steady-state mass transport limited current densities (j_L) at constant potential had to be determined quickly as function of rotation rate. The diffusion coefficient $D, \mathrm{HPbO_2^-}$ was derived as 0.61×10^{-9} m^2 s^{-1} from Levich's equation:

$$j_L(\mathrm{HPbO_2^-}) = 1.554\, nFD_{\mathrm{HPbO_2^-}}^{2/3} \nu^{-1/6} [\mathrm{HPbO_2^-}] f^{1/2} \quad (19)$$

This value was slightly larger than $D, \mathrm{Pb^{2+}} = 0.57 \times 10^{-10}$ m^2 s^{-1} derived from similar measurements in acidic electrolytes, presumably due to the greater degree of hydration of cations than anions, in spite of the intrinsically larger hydroxy complexes formed in alkaline media. Figure 7 shows corresponding voltammograms for Pb(II) oxidation at a Pt rotating disc electrode in 0.1 mol Pb(II) + 10 mol NaOH m^{-3}, which resulted in transport controlled current densities at about 0.75 V vs SCE and about 1.5 V vs SCE, respectively due to the reactions:

$$\mathrm{HPbO_2^- + OH^- \rightarrow PbO_2 + H_2O + 2e^-} \quad (7)$$

$$\mathrm{4OH^- \rightarrow O_2 + 2H_2O + 4e^-} \quad (8)$$

Oxygen evolution by decomposition of water occurred at higher potentials than the positive potential limit used in Figure 7. X-ray diffraction was used to confirm that the anodically deposited product layer was α-PbO_2; this was not as adherent and coherent as the β-PbO_2 formed in acidic electrolytes.

3.3. *Microkinetic modelling*

The potential dependences of current densities and efficiencies were estimated as functions of Pb(II) concentration and pH, using both thermodynamic information, such as shown in Figure 5, and kinetic data from the experimental results described above, or from the literature where available. This information was used to focus experimental work on conditions likely to lead to optimal reactor performance.

Literature values of the kinetic parameters for each reaction (7–11) were substituted in the extended Butler–Volmer equation for the kinetics of a simple redox reaction involving oxidized (O) and reduced (R) states, allowing for mass transport limitations and assuming an excess of supporting electrolyte to minimize migrational transport of the reactants, if charged:

$$j = \frac{j_0\left[\exp\left\{\frac{(1-\alpha)n_iF}{RT}\eta\right\} - \exp\left\{-\frac{\alpha n_iF}{RT}\eta\right\}\right]}{\left[1 + \left(\frac{j_0}{j_{\mathrm{L,R}}}\right)\exp\left\{\frac{(1-\alpha)n_iF}{RT}\eta\right\} + \left(\frac{j_0}{j_{\mathrm{L,O}}}\right)\exp\left\{-\frac{\alpha n_iF}{RT}\eta\right\}\right]} \quad (20)$$

This enabled prediction of the partial and total current density–electrode potential behaviour and hence of the potential dependence of the current efficiency (Φ_e) for Reactions 7 and 9. Values of exchange current densities (j_0) from the literature were modified for a range of solution compositions for each of the redox couples (O/R):

$$j_0 = nFk_0[\mathrm{O}]^{(1-\alpha)}[\mathrm{R}]^{\alpha} \tag{21}$$

In the first instance, the partial current densities due to the three cathodic reactions 9, 10 and 11, and for the anodic reactions 7 and 8, were assumed to be simply additive, involving no chemical interactions at each electrode, for example, in terms of the surface coverage of intermediates. Effects of bubble evolution could be added to allow for mass transport enhancement for partial current densities for hydrogen and oxygen evolution by Reactions 11 and 8.

The oxygen evolution reaction on α-PbO_2 in alkaline solutions exhibited a Tafel slope of 59 mV, half that in acid electrolytes, with an exchange current density (j_0) of 1.6×10^{-9} A m^{-2} in 10^{-2} M NaOH, and may be mass transport controlled with respect to hydroxide ions, depending on the potential. Current densities for reduction of dissolved oxygen on lead were measured experimentally and found to be transport controlled for potentials <-0.6 V vs SCE. Reaction 10 and/or

$$\mathrm{O_2 + H^+ + 2e^- \rightarrow H_2O} \tag{22}$$

could have been involved, so the parameters in the kinetic model were adjusted to give the same transport limited current densities as determined experimentally. In the envisaged process, were anodically-evolved oxygen to be reduced at cathode surfaces, severe losses in cathodic current efficiencies for Pb electrodeposition are predicted [8], especially as the concentration of Pb(II) decreases, since Reactions 9 and 10 are both transport controlled.

For hydrogen evolution in alkaline solutions (0.5 M NaOH), an exchange current density [12] of $j_0 = 3.4 \times 10^{-3}$ A m^{-2} and Tafel slope of 0.129 V decade^{-1} was used.

Figure 8 shows predictions for the kinetics of Reactions 9 and 7, using the following exchange current densities for the particular concentrations assumed: $j_0(\mathrm{Pb}) = 1$ A m^{-2} and $j_0(\mathrm{PbO_2}) = 10$ A m^{-2}, with corresponding Tafel slopes of 39 and 9.5 V^{-1}, respectively, which are typical of corresponding data for acidic electrolytes, no relevant data having been found in the literature for alkaline electrolytes. As these parameters have yet to be determined experimentally, the results in Figure 8 should be treated as illustrative only, though the variation of the exchange current densities by orders of magnitude had little impact on the potential dependence of current efficiencies, nor did variation of Tafel slopes from 10–60 V^{-1}.

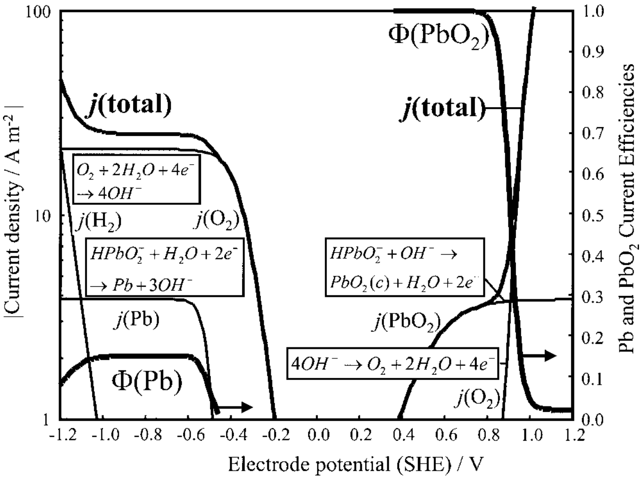

Fig. 8. Predicted kinetics of Pb(II) + O_2 reduction and Pb(II) + OH^- oxidation 1 mol Pb(II) + 1.3 mol O_2 m^{-3}, pH 12, RDE 16 Hz.

As the reversible potential for the latter reaction is more negative than that for oxygen evolution by Reaction 8, and the latter reaction becomes transport controlled with respect to hydroxide ions, PbO_2 deposition was predicted to occur with current efficiencies near unity and at a transport controlled rate, in the potential window of 0.3 to 0.8 V vs SHE, above which current efficiencies decay sharply, due to Reaction 8. This is broadly congruous with the voltammetric results shown in Figure 7 and coulometric results reported previously [8]. Whilst equilibrium concentrations of dissolved oxygen can be predicted [8]:

$$\mathrm{O_2(g) \rightleftharpoons O_2(aq)} \tag{23}$$

$$[\mathrm{O_2(aq)}]/\mathrm{mol\ m^{-3}} \cong 1.35\ P(\mathrm{O_2}) \tag{24}$$

were electrolytes to be supersaturated with anodically-evolved oxygen, cathodic current efficiencies for lead would be even lower than predicted in Figure 8.

Elemental lead was notionally excluded from the system for potentials >-0.6 V vs SHE, although the kinetics of oxygen reduction were deemed to be occurring on a dissolving lead surface for the purposes of determining whether or not the rate would be transport controlled at <-0.6 V vs SHE, at which lead would be deposited. In the absence of data for oxygen reduction kinetics on such a surface, the exchange current density was varied with a Tafel slope of 120 mV decade^{-1}, to determine the range of j_0 values for which Reaction 10 was predicted to be transport controlled at the potential at which elemental lead deposition occurred by Reaction 9. This condition was met for $j_0(\mathrm{O_2}) > 10^{-7}$ A m^{-2} at pH 12, confirming the legitimacy of modelling the reductive depletion of Pb(II) at -0.8 V vs SCE in the presence of dissolved oxygen, as involving two parallel transport controlled processes [8].

For the particular exchange current densities, Tafel slopes and mass transport rate coefficients used, PbO_2 deposition was predicted to occur under transport control at potentials >0,8 V vs SHE, At the cathode, oxygen reduction was the dominant reaction, with lead deposition occurring at potentials −0.2 V vs SHE, resulting in a maximum current efficiency of about 0.2 that decayed at potentials <−0.5 V vs SHE, due to hydrogen evolution.

In the first instance, ignoring the effects of gas evolution on effective electrolyte conductivities, and assuming particular values of interelectrode gaps (g) and mean electrolyte conductivities (σ), then data such as in Figure 8 can be used to calculate current density dependences of cell voltages from:

$$U = -\left(E_{\mathrm{A}} + \eta_{\mathrm{A}} - E_{\mathrm{C}} - \eta_{\mathrm{C}} + \frac{jg}{\sigma}\right) \tag{25}$$

Hence, current density dependences of specific electrical energy consumptions (SEEC) can be derived from:

$$\mathrm{SEEC} = \frac{2FU}{3.6 \times 10^{6}(\Phi_{\mathrm{PbO_2}} + \Phi_{\mathrm{Pb}})}\,\mathrm{kW\ h\ (mol\ Pb(II))^{-1}} \tag{26}$$

Differences in anode and cathode potentials can be read as a function of total current density from Figure 8, then the last term (jg/σ) in Equation 25 added, to give cell voltages (U). Combining these data with Pb and PbO_2 current efficiency predictions enables the effect of current density on specific electrical energy consumptions (SEEC) to be determined, as shown in Figure 9, for the reactor, which, in this illustrative example, had the same hydrodynamic behaviour as a rotating disc electrode rotating at 16 Hz. The sharp increase in SEEC at $j > 24$ A m^{-2} is related to the limiting current density for oxygen reduction being exceeded, so that the cathode potential steps to lower values at which hydrogen evolution occurs, causing ohmic contributions and hence, cell voltages to increase, and current efficiencies to decrease. Hence, for the particular conditions chosen for the microkinetic measurements and modelling, an optimal specific electrical energy consumption of about 0.27 kW h (mol Pb(II))$^{-1}$ can be identified for current densities of about \$24 A m^{-2}. For a specific electrical energy cost of \$0.05 kW h^{-1}, this translates to specific electrical energy cost for the process of about \$65 (tonne Pb removed)$^{-1}$, compared with LME (www.lme.com) prices of about \$450 (tonne Pb)$^{-1}$.

3.4. *Electrochemical reactor with graphite felt electrodes*

Whereas differential cathode and anode areas to achieve differential current densities can be made readily with two-dimensional electrodes, the problem is more constrained with three-dimensional electrodes, for which availability of suitable materials with appropriate specific surface areas/porosities structures may be a limitation. However, as explained below, a Ti felt cathode (specific surface area 3285 m^{-1}) and graphite felt anode (specific surface area 64 000 m^{-1}) were used in the later experimental work. In addition, modelling of potential, current density and concentration distributions in the direction normal to the electrode faces is required to attempt to use differential electrode areas to optimize anode and cathode current efficiencies; this will be reported in a future publication [13].

Figure 10 shows a voltammogram of the graphite felt cathode of the reactor shown in Figure 2, complete with cation-permeable membrane; the reference electrode's Luggin probe was positioned at the face of the felt cathode closest to the anode (Figure 2), so that the local apparent electrode potential in that plane includes the potential drop in the electrode phase from the feeder electrode, as shown schematically in Figure 11. Quantification of that potential drop will be reported elsewhere [13, 14], with results of one-dimensional modelling of the

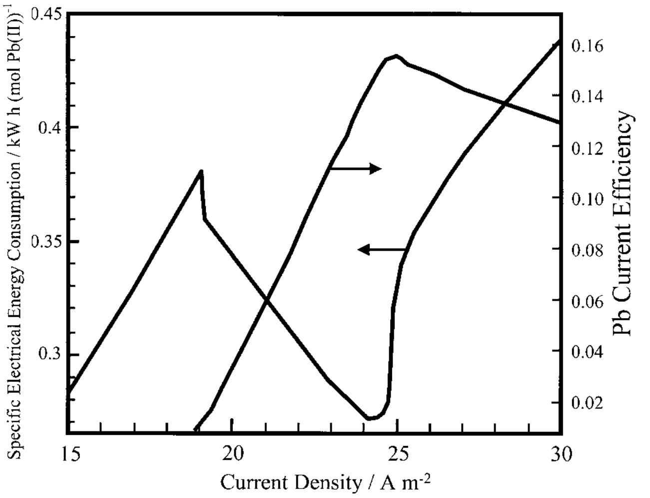

Fig. 9. Effect of current density on specific electrical energy consumption for Pb(II) deposition from $[HPbO_2^-] = 1$ mol m^{-3}, $[O_2] = 1.3$ mol m^{-3}, pH 12, electrolyte conductivity, $\sigma = 10$ S m^{-1}, gap 5 mm.

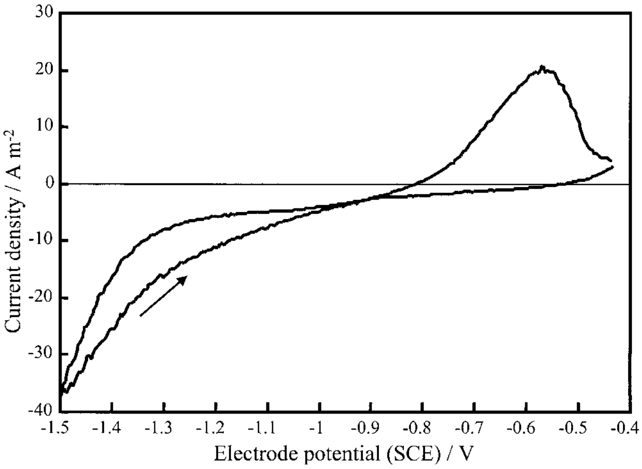

Fig. 10. Cyclic voltammogram of carbon felt electrode in 1 mol Pb(II) m^{-3} electrolyte at pH 13. Potential sweep rate 20 mV s^{-1} in membrane-divided reactor with electrolyte superficial velocity 6.3 mm s^{-1} and with N_2 bubbled through electrolyte in reservoir.

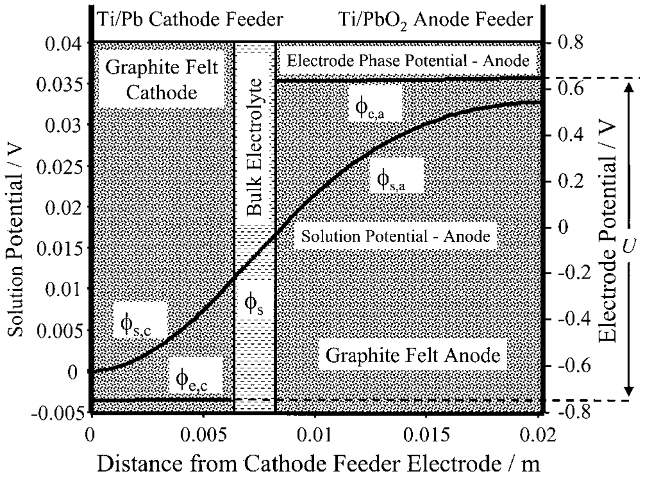

Fig. 11. Schematic potential distribution in electrochemical reactor with graphite felt anode (a) and cathode (c), operating with cell voltage *U*, and solution (ϕ_s) and electrode (ϕ_e) phase potentials, the controlled potential difference being between the cathode feeder electrode and the solution potential at the other extremity of the cathode felt.

potential, concentration, current density and current efficiency distributions in felt electrodes, together with specific electrical energy consumptions. As expected from Figure 6, what appeared to be transport controlled Pb(II) reduction by Reaction 9 occurred during the negative-going potential sweep in the range −1.0 to −1.3 V vs SCE, below which hydrogen partial current densities increased significantly. The significantly greater current densities on the positive-going potential sweep from the negative potential limit resulted from the time-dependent electrode area. At potentials >−0.8 V vs SCE, stripping of the Pb electrodeposit occurred by the reverse of Reaction 9, giving rise to the current peak at about −0.6 V vs SCE.

Figure 12 shows the time dependence of the Pb(II) concentration in the anolyte, together with the incremental and cumulative charge efficiencies for Reaction 7, at a constant anode potential corresponding to a value on the mass transport controlled plateau in Figure 7, though not allowing for potential losses. The anode felt was three times the thickness of the cathode, to try to optimise anode and cathode current efficiencies, as discussed above.

For a single mass transport controlled reaction in a plug flow reactor operated in batch recycle mode with a stirred tank reservoir, the reactant concentration c_t is predicted to decay exponentially with time t, according to [15]:

$$c_t = c_{t=o}\exp\left\{-\frac{ut}{V}\left[1-\exp\left(-\frac{\bar{k}_{\mathrm{m}}AaL}{u}\right)\right]\right\} \tag{27}$$

Though the form of the limited data for concentration decay in Figure 12 deviates significantly from the theoretical prediction of Equation 27 at the lowest concentration, the value of $k_{\mathrm{m}}AaL$ fitted to the dashed line corresponds to a value of 8×10^{-6} m^3 s^{-1}. This is in broad agreement with data reported in the literature [16–18] for transport controlled reactions with similar materials. The decreasing gradient of the log concentration–time data with increasing time in Figure 12 may have resulted from the increasing reversible potential with decreasing concentration, causing decreasing overpotentials within the anode, so that not all its volume was operating under transport control. In addition, the anode's active area changed with time due to PbO$_2$ deposition, as shown in the photomicrograph in Figure 14. Also, it is probable that the active area changed with time due to bubbles blinding surfaces at which oxygen gas evolution occurred; the detrimental effects of bubbles in three dimensional electrodes [19] has been reported for hydrogen evolution in parallel with zinc deposition. Nonetheless, Figure 12 shows that Pb(II)

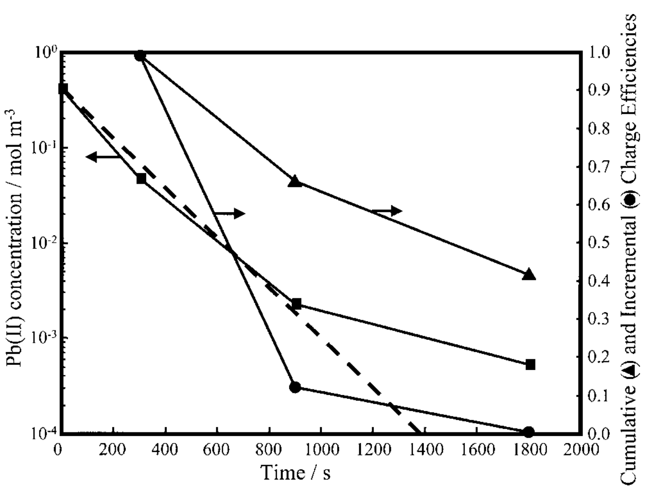

Fig. 12. Time-dependence of Pb(II) concentration and charge efficiency for Pb(II) oxidation at 0.72 V vs SCE in 1 dm^3 electrolyte of pH 13 in batch recycle reactor with 18 mm thick C felt anode +6 mm cathode with cation-permeable membrane.

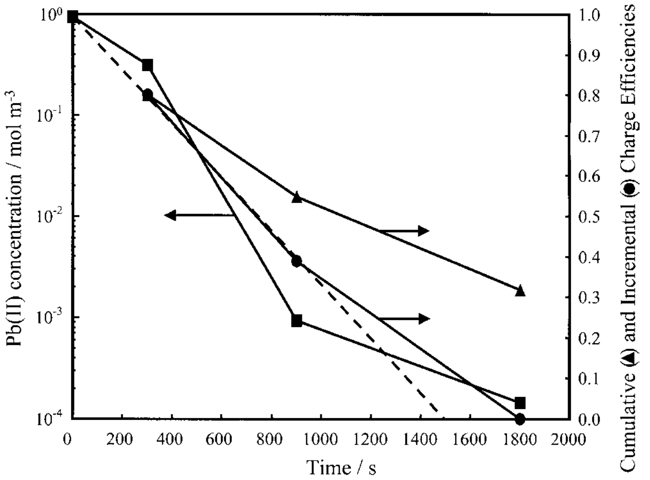

Fig. 13. Time dependence of Pb(II) concentration and charge efficiency for Pb(II) reduction at about −2 V vs SCE in 1 dm^3 electrolyte of pH 13 in reactor with 18 mm thick graphite felt anode +6 mm cathode, operated in batch recycle mode with membrane. (Initial anode potential 0.96 V vs SCE).

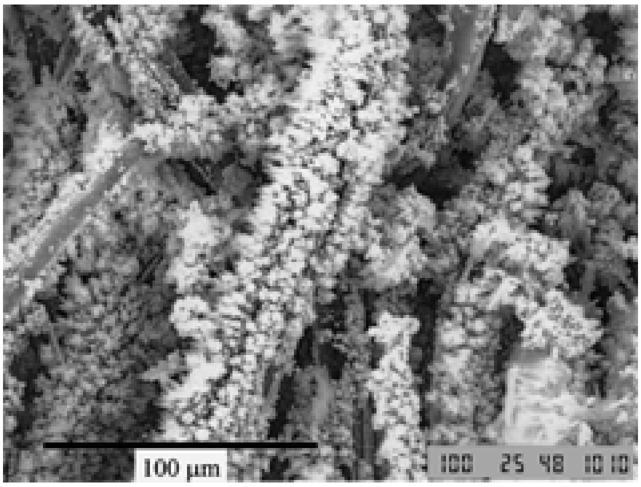

Fig. 14. Photomicrograph of Pb electrodeposited on graphite felt cathode in pH 13 aq. NaOH + 10^{-3} M Pb(II).

was depleted to subanalytically detectable concentrations, though with incremental charge efficiencies that predictably also decreased, as oxygen evolution partial current densities due to Reaction 7 became dominant.

Figure 13 shows the corresponding time dependence of Pb(II) concentration and charge efficiency for Pb(II) reduction at the exceptionally low potential of about −2 V vs SCE, to try to ensure that the whole cathode volume was operated under transport control; again, this potential difference included the ohmic potential drop in the electrolyte (Figure 11). Even so, cumulative charge efficiencies were about 0.3 to deplete Pb(II) from an initial concentration of about 1 mol m^{-3} by almost four orders of magnitude, to the limit detectable by ICP spectroscopy. Incremental charge efficiencies decreased from an initial value of about 0.8 to zero, as oxygen reduction (Reaction 10) and hydrogen evolution (Reaction 11) partial current densities became dominant. The photomicrograph in Figure 15 shows a more compact structure for the elemental lead deposit compared with that for α-PbO_2 shown in Figure 14; conversely, at low pH, β-PbO_2 forms a more compact deposit on the anode than does elemental lead on the cathode.

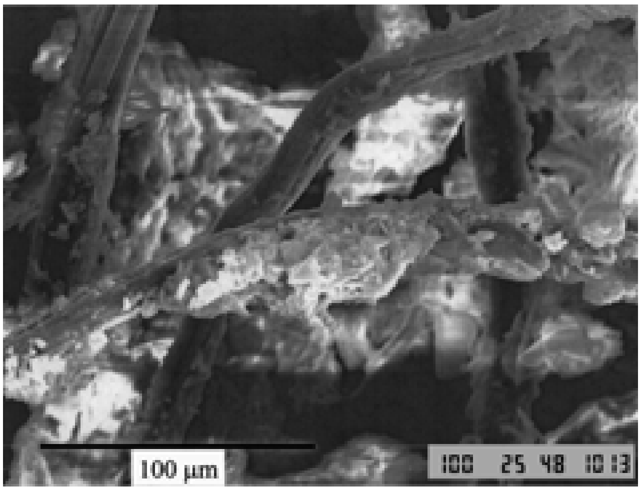

Fig. 15. Photomicrograph of α-PbO_2 on graphite felt anode in pH 13 aq. NaOH + 10^{-3} M Pb(II).

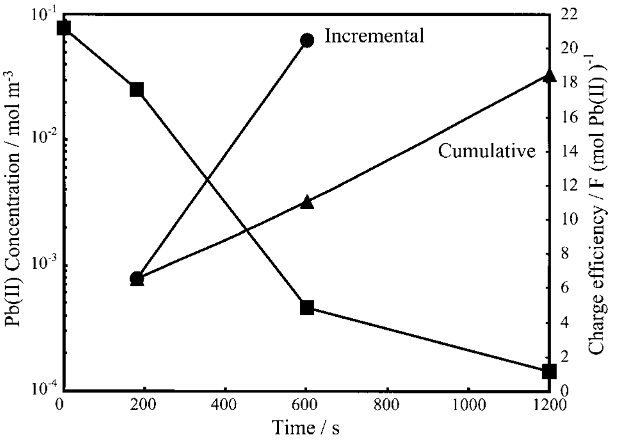

Fig. 16. Time-dependence of Pb(II) concentration and charge efficiencies for Pb(II) removal in undivided tubular reactor with 2 mm × 6.3 mm thick graphite felt anode and 6 mm thick Ti felt cathode, using 2 dm^3 of industrial effluent at pH 11.5 with superficial velocity of 6.3×10^{-3} m s^{-1} and applied cathode potential between Ti feeder electrode and reference electrode of −1.4 V vs SCE.

Finally, the membrane was removed and a titanium felt cathode was used, with a specific surface area about twenty times smaller than the graphite felt used as the anode, again in an attempt to optimise cathode and anode current efficiencies. Figure 16 shows the resulting time dependence of the Pb(II) concentration in the treatment of an industrial effluent at pH 11.5 and using a cathode potential of −1.4 V vs SCE, Pb(II) concentrations again decaying rapidly to subanalytically detectable concentrations. Using the number (x) of F (mol Pb(II) removed)$^{-1}$, rather than charge efficiency, as the figure of merit for the undivided reactor, the specific electrical energy consumption (SEEC) is then defined by

$$\mathrm{SEEC} = \frac{xFU}{3.6 \times 10^6} \quad \mathrm{kW\ h\ (mol\ Pb(II))^{-1}} \qquad (28)$$

Were both anode and cathode to operate at charge efficiencies of unity for Pb(II) removal by Reactions 7 and 9, then according to Equation 26, the reactor would require 1 faraday per mole of Pb(II) removed. Figure 16 indicates an actual cumulative specific charge requirement of 6.5 increasing to 18.5 F (mol Pb(II))$^{-1}$, as the Pb(II) concentration decayed from 0.75×10^{-2} to 1.4×10^{-4} mol m^{-3}, and the kinetics of loss Reactions 8, 10 and 11 became dominant. The cell voltage decayed from 3.2 to 2.6 V, corresponding to 2.7 to 8.0 MW h (tonne Pb(II) removed)$^{-1}$.

When nitrogen was bubbled into the reservoir of the batch recirculation system shown schematically in Figure 2, the decrease in dissolved oxygen concentration and hence in the rate of loss reaction (10), greatly decreased the reactor specific charge requirement, as demonstrated by comparison of Figure 17 with Figure 16. Specific electrical energy consumptions corresponding to the data in Figure 17 were 1.4 to 3.1 MW h (tonne Pb(II) removed)$^{-1}$.

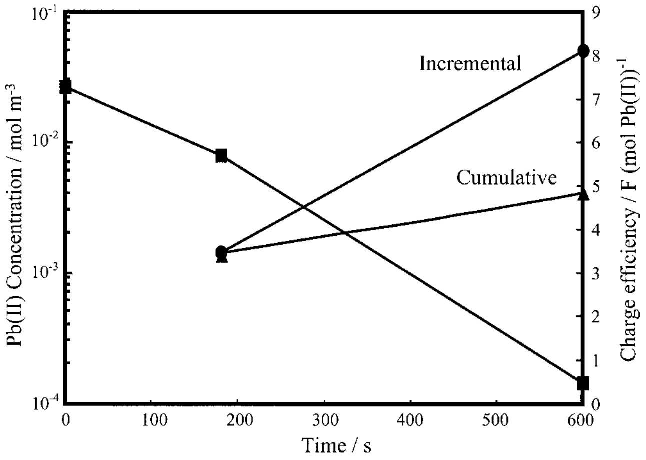

Fig. 17. Time-dependence of Pb(II) concentration and charge efficiencies for Pb(II) removal in undivided tubular reactor with 2 mm × 6.3 mm thick graphite felt anode and 6 mm thick Ti felt cathode, using 2 dm^3 of deoxygenated industrial effluent at pH 11.5 with superficial velocity of 6.3×10^{-3} m s^{-1} and applied cathode potential between Ti feeder electrode and reference electrode of −1.4 V vs SCE.

4. Conclusions

- (i) Effects of pH and [sulfate] on Pb(II) solubilities have been predicted from published thermodynamic data.
- (ii) With sufficient overpotentials, the kinetics of Pb(II) oxidation and reduction are transport controlled, with high efficiencies for PbO_2 deposition, but [O_2 (aq)] limits efficiencies for Pb deposition, especially at high Pb(II) conversions.
- (iii) Modelling electrochemical (micro) kinetics enabled predictions of current efficiencies and specific electrical energy consumptions for Pb(II) reduction and oxidation, separately and combined.
- (iv) Pb(II) concentrations were depleted to <60 ppb in a batch recycle reactor system with graphite felt anodes and graphite or titanium felt cathodes. Simultaneous cathodic Pb and anodic PbO_2 electrodeposition resulted in more rapid Pb(II) depletion than for either reaction separately.

Acknowledgement

The authors thank the UK Engineering and Physical Sciences Research Council for a grant, providing a research fellowship for Q.Y.

References

1. K. Ramus and P. Hawkins, *J. Power Sources* **42** (1993) 299.
2. C.P. de Leon and D. Pletcher, *Electrochim. Acta* **41** (1996) 533.
3. A. Czerwinski and M. Zelazowska, *J. Electroanal. Chem.* **410** (1996) 55.
4. A. Czerwinski and M. Zelazowska, *J. Power Sources* **64** (1997) 29.
5. R.C. Widner, M.F.B. Sousa and R. Bertazzoli, *J. Appl. Electrochem.* **28** (1999) 201.
6. M.S. El-Deab, M.M. Saleh, B.E. El-Anadouli and B.G. Ateya, *J. Electrochem. Soc.* **146** (1999) 208.
7. G. Carreno, E. Sosa, I. Gonzalez, C. Ponce-de-León, N. Batina and M.T. Oropeza, *Electrochim. Acta* **44** (1999) 2633.
8. N.P. Brandon, G.H. Kelsall and Q. Yin, 200th Electrochemical Society Meeting, San Francisco, 2–7 Sept. 2001 and *in* C. Comninellis, M. Doyle and J. Winnick (Eds), 'Energy and Electrochemical Processes for a Cleaner Environment', *Proc. Electrochem. Soc.* Vol. 2001–23 (Electrochemical Society, NJ, 2001), pp. 306-322.
9. Z. Galus, *in* A.J. Bard, R. Parsons and J. Jordan (Eds), 'Standard Potentials in Aqueous Solutions' (Marcel Dekker, New York, 1985), pp. 220–235.
10. D.D. Wagman, W.H. Evans, V.B. Parker, R.H. Schumm, I. Halow, S.M. Bailey, K.L. Churney and R.L. Nuttall, 'The NBS Tables of Chemical Thermodynamic Properties', *J. Phys. Chem. Ref. Data* **11** (Supplement 2) (1982) 2–219.
11. G.H. Kelsall and F.P. Gudyanga, *J. Electroanal. Chem.*, to be submitted.
12. J.O'M. Bockris and S. Srinivasan, *Electrochim. Acta* **9** (1964) 31.
13. D. Pilone and G.H. Kelsall, *in* F. Doyle, G.H. Kelsall and R. Woods (Eds), 'Electrochemistry in Mineral and Metal Processing VI', **PV-2003** (Electrochemical Society Proceedings Series, Pennington, NJ 2003), in press.
14. D. Pilone and G.H. Kelsall, *J. Electrochem. Soc.*, to be submitted.
15. A.T.S. Walker and A.A. Wragg, *Electrochim. Acta* **22** (1977) 1129.
16. P.N. Dweivedi and S.N. Upadhyay, *Ind. Eng. Chem., Process Des. Dev.* **16** (1977) 157.
17. R. Carta, S. Palmas, A.M. Polcaro and G. Tola, *J. Appl. Electrochem.* **21** (1991) 793.
18. N. Vatista, P.F. Marconi and M. Bartolozzi, *Electrochim. Acta* **36** (1991) 339.
19. M.M. Saleh, J.W. Weidner and B.G. Ateya, *J. Electrochem. Soc.* **142** (1995) 4113.